


\mathcal{PT} -symmetry-breaking-enhanced cavity optomechanical magnetometryZhucheng Zhang ¹, Yi-Ping Wang,² and Xiaoguang Wang^{1,3,*}¹*Zhejiang Institute of Modern Physics, Department of Physics, Zhejiang University, Hangzhou 310027, China*²*College of Science, Northwest A&F University, Yangling 712100, China*³*Graduate School of China Academy of Engineering Physics, Beijing 100193, China*

(Received 23 March 2020; accepted 17 July 2020; published 7 August 2020)

A \mathcal{PT} -symmetry-breaking-enhanced cavity optomechanical magnetometer is proposed, which is achieved by monitoring the change in intensity of a nonlinear four-wave mixing (FWM) process in a gain-cavity-assisted cavity optomechanical system (COMS). Compared with the traditional single loss COMS, the FWM intensity can be enhanced by two orders of magnitude when the gain-cavity-assisted COMS operates on the \mathcal{PT} -symmetry-breaking phase. Meanwhile, the sensitivity of magnetic-field sensing can be increased from 10^{-9} T to 10^{-11} T. This originally comes from the fact that the effective detuning and decay of the loss cavity can be effectively modified in the \mathcal{PT} -symmetry-breaking phase. Our work shows that an ultrahigh-sensitivity magnetometer can be achieved in the \mathcal{PT} -symmetry-breaking COMS, which will have wide applications in the field of quantum sensing.

DOI: [10.1103/PhysRevA.102.023512](https://doi.org/10.1103/PhysRevA.102.023512)**I. INTRODUCTION**

Ultrahigh-sensitivity magnetometers with small size play an important role in medicine, geology, biology, defense, and so on [1–4], which attracts great interest from researchers. Although the sensitivity of magnetometers based on atom and magnetostrictive material can achieve a magnitude of aT Hz^{-1/2} and fT Hz^{-1/2}, the size scale of these systems are generally limited to millimeters or centimeters [5,6]. Besides, magnetometers based on superconducting quantum interference devices and nitrogen vacancy centers are hampered by operating temperature, fabrication issues, and read-out schemes, respectively [2,7–9]. To improve the sensitivity and reduce the size of the magnetometer is still the focus of designing systems.

Cavity optomechanics is a hot research field exploring the nonlinear interaction between electromagnetic radiation and nano- and micromechanical systems [10], which provides a promising platform for much theoretical and experimental research, such as quantum ground-state cooling of mechanical oscillators [11–13], optomechanically induced transparency [14–16], normal-mode splitting [17–20], and so on. With this nonlinear optomechanical interaction, a micron-scale cavity optomechanical magnetometer with room-temperature operation has realized a peak magnetic-field sensitivity of 400 nT Hz^{-1/2} via the magnetic-field-induced deformations of a magnetostrictive material in experiment [21]. Besides, it has been shown that thanks to this nonlinear interaction, the lower and upper motional sidebands can be generated in the transmission spectra of cavity optomechanical systems (COMSs) [13,22]. Based on these motional sidebands, the weak magnetic field can also be precisely measured by find-

ing out the correlations between the structure of transmission spectra and the measured magnetic field. For example, through monitoring the deformation of an optomechanically induced transparency window (corresponding to the upper first-order sideband) [23], or the change of intensity of the upper second-order sideband [24], cavity optomechanical magnetometers can achieve a sensitivity of nT through electromagnetic interactions in theories. Furthermore, utilizing these motional sidebands, COMS can also be used to sense other physical quantities, such as electrical charges [25,26], environmental temperature [27], mass [28–30], and so on. For the COMS as an all-optical sensor, these motional sidebands are undoubtedly a powerful tool.

On the other hand, since the concept of parity-time (\mathcal{PT}) symmetry was put forward, it has been widely studied in theories and experiments [31], such as for \mathcal{PT} -symmetric phonon lasers [32], \mathcal{PT} -symmetry-breaking chaos [33], loss-induced transparency [34], low-power optical diodes [35], and single-mode lasers [36,37]. With the singular characteristics of \mathcal{PT} -symmetric systems operating at the phase transition from unbroken to broken \mathcal{PT} symmetry, \mathcal{PT} -symmetric systems can be used as sensors for acoustics [38] and mechanical motion [39]. In addition, the concept of \mathcal{PT} symmetry was introduced into quantum noise theory to calculate the signal-to-noise performance [40]. Recently, the generation of motional sidebands has been shown to be enhanced in \mathcal{PT} -symmetric COMSs [41]. Thus, a natural question is whether a \mathcal{PT} -symmetric COMS combined with motional sidebands can significantly enhance the sensitivity of magnetic-field sensing, which will be a significant improvement for a magnetometer based on COMSs.

In this paper, we propose a \mathcal{PT} -symmetry-breaking-enhanced cavity optomechanical magnetometer by monitoring the change of intensity of the lower first-order sideband in a gain-cavity-assisted cavity optomechanical system, which

*xgwang1208@zju.edu.cn

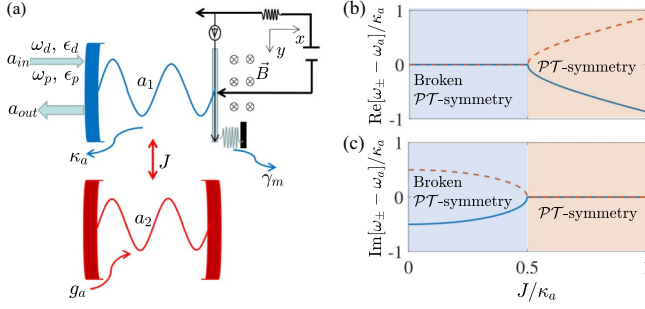


FIG. 1. (a) Schematic diagram of a \mathcal{PT} -symmetric COMS, in which a loss COMS [with decay rate κ_a (γ_m) of cavity (mechanical) mode] is coupled to a gain cavity (with optical gain rate g_a of cavity mode) by photon hopping with strength J . Besides, the loss COMS is driven by a strong driving field of frequency ω_d with amplitude ϵ_d and probed by a weak probe field of frequency ω_p with amplitude ϵ_p . Meanwhile, the movable end (as an electromechanical oscillator) is passed through a surface current with intensity I and the measured magnetic field with strength B is applied to the loss COMS. a_{in} (a_{out}) is the input (output) of the loss cavity. (b), (c) Real and imaginary parts of the eigenfrequencies ω_+ and ω_- of the two supermodes as a function of the coupling parameter J . The gain-cavity-assisted COMS with balanced gain g_a and loss κ_a can show a phase transition from broken to unbroken \mathcal{PT} symmetry by controlling the coupling parameter J .

corresponds to a nonlinear four-wave mixing (FWM) process [42]. Compared with the traditional single-loss COMS, we show that the FWM intensity in the \mathcal{PT} -symmetric COMS can be enhanced by two orders of magnitude. What is more, the measurement precision of a weak magnetic-field based on the change of FWM intensity can be increased from 10^{-9} T to 10^{-11} T. Physically, when the \mathcal{PT} -symmetry-breaking phase occurs, the effective decay of the loss cavity can be completely balanced by the optical gain of the gain cavity, meanwhile, the effective detuning of the loss cavity can also be effectively modified by the electromagnetic interaction. These ultimately lead to the result that the sensitivity of the \mathcal{PT} -symmetric COMSs can be higher than the traditional single-loss COMSs. This unconventional optomechanical magnetometer combines \mathcal{PT} symmetry and motional sidebands, which will have wide applications in the field of precision measurement.

This paper is organized as follows: In Sec. II, we introduce the theoretical model of the \mathcal{PT} -symmetric COMS and derive its dynamical equations. In Secs. III and IV, we discuss in detail the performance of magnetic-field sensing in this system through monitoring the change of intensity of the FWM process and compare it with the case of the traditional single-loss COMSs. In Sec. V, we analyze the improvement of magnetic-field sensing based on the \mathcal{PT} -symmetric COMS. Finally, we summarize our conclusions in Sec. VI.

II. THEORETICAL MODEL

The proposed \mathcal{PT} -symmetric COMS is shown in Fig. 1(a), in which the measured weak magnetic field is applied to our system through the electromagnetic interaction. The Hamilto-

nian of system can be written as

$$\begin{aligned}
 H = & -\hbar\Delta_a(a_1^\dagger a_1 + a_2^\dagger a_2) + \frac{p^2}{2m} + \frac{1}{2}m\omega_m^2 x^2 \\
 & + \hbar J(a_1^\dagger a_2 + a_2^\dagger a_1) + \hbar G a_1^\dagger a_1 x + \zeta B x \\
 & + i\hbar\sqrt{\eta_c\kappa_a}[(\epsilon_d a_1^\dagger + \epsilon_p a_1^\dagger e^{-i\Omega t}) - \text{H.c.}], \quad (1)
 \end{aligned}$$

in which a_1 (a_1^\dagger) and a_2 (a_2^\dagger) are the annihilation (creation) operators of the loss cavity and the gain cavity, respectively. $\Delta_a = \omega_d - \omega_a$ and $\Omega = \omega_p - \omega_d$ are the frequency detunings with the cavity resonance frequency ω_a . p (x) is the momentum (position) operator of the oscillator (with resonance frequency ω_m and mass m). J represents the coupling strength between the loss and gain cavities, which can be controlled by changing the distance between the two cavities. The term $\hbar G a_1^\dagger a_1 x$ characterizes the optomechanical interaction between the loss cavity and the oscillator with coupling strength G . The parameter ζ represents the strength of electromagnetic interaction, which is proportional to the current intensity I and the effective range of action. The last term describes the interactions between the input fields and the loss cavity with a critical coupling parameter $\eta_c = 1/2$. $\epsilon_{d,p} = \sqrt{P_{d,p}/\hbar\omega_{d,p}}$ is the amplitude of the input fields with power $P_{d,p}$ and frequency $\omega_{d,p}$, and κ_a is the total decay rate of the loss cavity.

With the semiclassical Langevin equations [i.e., setting $o(t) \equiv \langle o(t) \rangle$, $o = a_1, a_2, x, p$], the dynamics evolution of system can be described by the following equations:

$$\begin{aligned}
 \frac{da_1}{dt} = & \left(i\Delta_a - iGx - \frac{\kappa_a}{2}\right)a_1 - iJa_2 \\
 & + \sqrt{\eta_c\kappa_a}(\epsilon_d + \epsilon_p e^{-i\Omega t}), \quad (2)
 \end{aligned}$$

$$\frac{da_2}{dt} = \left(i\Delta_a + \frac{g_a}{2}\right)a_2 - iJa_1, \quad (3)$$

$$\frac{d^2x}{dt^2} = -\gamma_m \frac{dx}{dt} - \omega_m^2 x - \frac{1}{m}(\hbar G a_1^\dagger a_1 + \zeta B), \quad (4)$$

in which g_a is the gain rate of the gain cavity. In our system, the coupling between loss and gain cavities leads to two supermodes, and their eigenfrequencies ω_+ and ω_- can be obtained by diagonalizing the corresponding coefficient matrix of Eqs. (2) and (3) under the weak-coupling regime [43,44]. For the \mathcal{PT} -symmetric COMS with balanced gain and loss, the eigenfrequencies of the two supermodes in the frame of the cavity frequency ω_a can be derived as $\omega_\pm = \omega_a \pm (J^2 - \kappa_a^2/4)^{1/2}$. As shown in Figs. 1(b) and 1(c), when the coupling parameter $J = 0.5\kappa_a$, the gain-cavity-assisted COMS with balanced gain and loss can show a \mathcal{PT} -symmetry phase transition, in which the two eigenfrequencies coalesce [31], i.e., $\omega_+ = \omega_- = \omega_a$. One can find in the following sections that the system can show a better sensitivity for the change of weak magnetic field at this \mathcal{PT} -symmetry-breaking point.

Due to the fact that the probe field is much weaker than the driving field, the above dynamic equations can be solved by the perturbation method. Using $o = o_s + \delta o$ with o_s and δo being the steady-state values and the corresponding perturbation

terms, respectively, one can get the following steady-state values:

$$a_{1s} = -\frac{\sqrt{\eta_c \kappa_a} \epsilon_d}{i\Delta_{\text{eff}} - \frac{\kappa_{\text{eff}}}{2}}, \quad a_{2s} = \frac{iJa_{1s}}{i\Delta_a + \frac{g_a}{2}}, \quad (5)$$

$$x_s = -\frac{\hbar GN_1 + B\zeta}{m\omega_m^2}, \quad (6)$$

with the effective detuning Δ_{eff} and decay rate κ_{eff} of the loss cavity due to the three interactions in our system, i.e., optomechanical, electromagnetic, and double-cavity interactions,

$$\Delta_{\text{eff}} = \Delta_a - [Gx_s + J^2 \Delta_a / (\Delta_a^2 + g_a^2/4)], \quad (7)$$

$$\kappa_{\text{eff}} = \kappa_a - J^2 g_a / (\Delta_a^2 + g_a^2/4), \quad (8)$$

and the average photon number of the loss cavity, $N_1 = |a_{1s}|^2$. One can find that the effective detuning Δ_{eff} and the effective decay rate κ_{eff} are related to the driving detuning Δ_a and the coupling parameter J .

Besides, the corresponding evolution of the perturbation terms can be derived as

$$\begin{aligned} \frac{d\delta a_1}{dt} &= \left(i\Delta - \frac{\kappa_a}{2}\right)\delta a_1 - iJ\delta a_2 \\ &\quad - iG(a_{1s}\delta x + \delta a_1\delta x) + \sqrt{\eta_c \kappa_a} \epsilon_p e^{-i\Omega t}, \end{aligned} \quad (9)$$

$$\frac{d\delta a_2}{dt} = \left(i\Delta_a + \frac{g_a}{2}\right)\delta a_2 - iJ\delta a_1, \quad (10)$$

$$\begin{aligned} \frac{d^2\delta x}{dt^2} &= -\gamma_m \frac{d\delta x}{dt} - \omega_m^2 \delta x \\ &\quad - \frac{\hbar G}{m}(a_{1s}\delta a_1^* + a_{1s}^*\delta a_1 + \delta a_1^*\delta a_1), \end{aligned} \quad (11)$$

in which $\Delta = \Delta_a - Gx_s$. To solve the above nonlinear equations, we make the following ansatz:

$$\delta a_1 = A_1^u e^{-i\Omega t} + A_1^l e^{i\Omega t}, \quad (12)$$

$$\delta a_2 = A_2^u e^{-i\Omega t} + A_2^l e^{i\Omega t}, \quad (13)$$

$$\delta x = X_1 e^{-i\Omega t} + X_1^* e^{i\Omega t}, \quad (14)$$

in which A_1^l (A_1^u) represents the coefficient of the lower (upper) first-order sideband of the loss COMS. We should note that our scheme focuses on the combined effects of the \mathcal{PT} symmetry and the lower first-order sideband on the weak magnetic-field sensing, which corresponds to a nonlinear four-wave mixing (FWM) process [13,22,42]. By substituting the ansatz into Eqs. (9)–(11), we can get the solution for A_1^l ,

$$A_1^l = \frac{ia_{1s}^2 \epsilon_p G^2 \hbar \sqrt{\eta_c \kappa_a}}{D(\Omega)}, \quad (15)$$

with

$$D(\Omega) = 2|a_{1s}|^2 G^2 \hbar D_1(\Omega) + mD_2(\Omega)D_3(\Omega)D_4(\Omega), \quad (16)$$

$$D_1(\Omega) = \Delta - \frac{\Delta_a J^2}{\Delta_a^2 - \left(i\frac{g_a}{2} + \Omega\right)^2}, \quad (17)$$

$$D_2(\Omega) = \left[\Delta + \left(i\frac{\kappa_a}{2} - \Omega\right)\right] - \frac{J^2}{\Delta_a - \left(i\frac{g_a}{2} + \Omega\right)}, \quad (18)$$

$$D_3(\Omega) = \left[\Delta - \left(i\frac{\kappa_a}{2} - \Omega\right)\right] - \frac{J^2}{\Delta_a + \left(i\frac{g_a}{2} + \Omega\right)}, \quad (19)$$

$$D_4(\Omega) = \omega_m^2 - \Omega^2 + i\gamma_m \Omega. \quad (20)$$

Then, based on the input-output relation of the cavity, i.e., $a_{\text{out}} = a_{\text{in}} - \sqrt{\eta_c \kappa_a} a_1$, the output field of our system can be obtained as [14,45]

$$\begin{aligned} a_{\text{out}}(t) &= \underbrace{(\epsilon_d - \sqrt{\eta_c \kappa_a} a_{1s}) e^{-i\omega_d t}}_{\text{Driving field}} + \underbrace{(\epsilon_p - \sqrt{\eta_c \kappa_a} A_1^u) e^{-i\omega_p t}}_{\text{Probe field}} \\ &\quad - \underbrace{\sqrt{\eta_c \kappa_a} A_1^l e^{-i(2\omega_d - \omega_p)t}}_{\text{FWM field}}, \end{aligned} \quad (21)$$

which clearly shows that, in addition to the driving and probe fields, the FWM field with frequency $2\omega_d - \omega_p$ and intensity $|\sqrt{\eta_c \kappa_a} A_1^l|^2$ can be generated in our system.

In addition, according to the expression of A_1^l , i.e., Eq. (15), one can find that it is useful to normalize the intensity of FWM to that of the input probe field, $|\epsilon_p|^2$. Thus, the intensity of FWM in terms of the input probe field can be defined as [14,19]

$$I_{\text{FWM}} = \left| \frac{\sqrt{\eta_c \kappa_a} A_1^l}{\epsilon_p} \right|^2, \quad (22)$$

which is a dimensionless quantity. The optical response in optomechanics can be detected in experiments, such as the homodyne detection scheme in Ref. [14].

III. MAGNETIC-FIELD SENSING WITH A SINGLE-LOSS CAVITY OPTOMECHANICAL SYSTEM

At first, we study the performance of magnetic-field sensing based on the change of FWM intensity with a single-loss COMS. The parameters used in our numerical simulations are analogous to the related theoretical and experimental works [23,24,46]. As shown in Figs. 2(a) and 2(b), the FWM intensity spectrum is plotted as a function of the detuning Ω . In our scheme, the loss COMS is driven resonantly, which can significantly enhance the intensity of FWM compared with the red- and blue-detuning, as shown in Fig. 2(a). With the resonantly driven single-loss COMS, one can find that the intensity of FWM decreases with the increase of the measured weak magnetic field [see Fig. 2(b)]. Meanwhile, the sensitivity of this system can distinguish the magnetic field with only about 10^{-9} T. Physically, for the resonantly driven single loss COMS, the effective detuning Δ_{eff} of the loss cavity is simplified as $-Gx_s$. Due to the presence of the optomechanical interaction, the value of the effective detuning is not zero [see the inset of Fig. 2(c)], but with the increase of the measured magnetic field, it quickly decreases to zero at first, then its absolute value increases gradually, which shows that the driving of the single loss COMS deviates from the resonance condition gradually even if there is a small region close to resonance. Besides, from Fig. 2(d), one can find that, due to the small region close to resonance of the effective detuning, the average photon number of the loss cavity slightly increases at first, but it also gradually decreases, which is consistent with the change trend of the effective

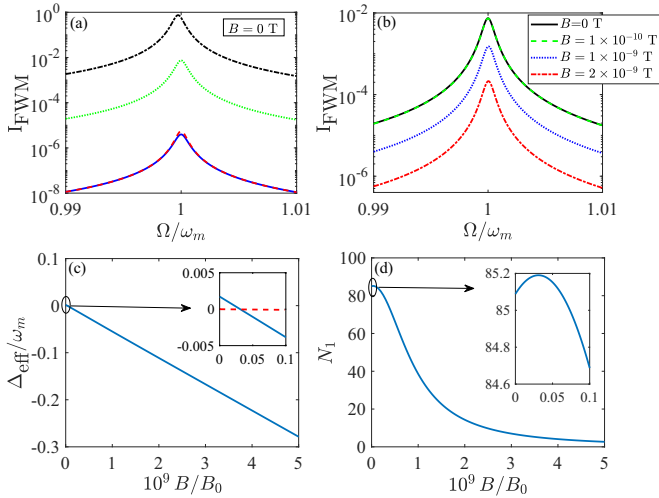


FIG. 2. (a), (b) FWM intensity spectrum as a function of detuning Ω . (a) The solid blue and dashed red curves represent the loss cavity driven by blue detuning (i.e., $\Delta_a = \omega_m$) and red detuning (i.e., $\Delta_a = -\omega_m$), respectively, and the coupling parameter $J = 0$. The dotted green and dot-dashed black curves represent the coupling parameter $J = 0$ and $J = 0.5\kappa_a$, respectively, and the loss cavity is driven resonantly, i.e., $\Delta_a = 0$. (b) The loss-cavity is driven resonantly, and the coupling parameter $J = 0$. The parameters are $B_0 = 1$ T, $\omega_m = 2\pi \times 0.1$ MHz, $m = 100$ pg, $G = -2\pi \times 11$ MHz/nm, $\gamma_m = 2\pi \times 0.1$ kHz, $\kappa_a = 0.1\omega_m$, $g_a = \kappa_a$, $\zeta = 2 \times 10^{-5}$ A m for the current intensity $I = 1$ mA, $P_d = 1$ pW, and the wavelength of the driving field $\lambda_d = 2\pi c/\omega_d = 532$ nm (c represents the speed of light in vacuum). (c) Effective detuning Δ_{eff} and (d) average photon number N_1 of the loss cavity as a function of strength B of the measured weak magnetic field with $J = 0$ and $\Delta_a = 0$.

detuning. This ultimately leads to the result that the FWM intensity generated in the single loss COMS decreases with the increase of the measured magnetic field, which also limits the performance of system for the magnetic-field sensing.

IV. MAGNETIC-FIELD SENSING WITH \mathcal{PT} -SYMMETRIC CAVITY OPTOMECHANICAL SYSTEM

Now we study the weak magnetic-field sensing based on a \mathcal{PT} -symmetric COMS. As shown in Fig. 2(a), one can find that the FWM intensity generated with the \mathcal{PT} -symmetric

COMS (see dot-dashed black curve) can be enhanced by two orders of magnitude compared with the resonantly driven single loss COMS (see dotted green curve), which will be easier to observe in experiments. Besides, as shown in Fig. 3(a), the FWM intensity spectrum is plotted as a function of the detuning for different magnetic-field strengths. From the curves, we can see that the FWM intensity increases with the increase of the magnetic field, which is opposite to the change trend of the resonantly driven single loss COMS. As expected, the \mathcal{PT} -symmetric COMS shows a higher sensitivity to the change of the weak magnetic field compared with Fig. 2(b). To better show the dependence of the FWM intensity on the measured magnetic field, we plot the maximum value I_{max} of the FWM intensity spectrum as a function of the magnetic-field strength, as shown in Fig. 3(b). From the inset of Fig. 3(b), one can see that the \mathcal{PT} -symmetric COMS can even distinguish the magnetic field with strength 10^{-11} T based on the change in the FWM intensity, which is increased by two orders of magnitude compared with the single loss COMS. Similarly, this enhanced sensitivity can be understood as follows: for the \mathcal{PT} -symmetry-breaking COMS, one can find that the effective decay rate of the loss cavity can be completely balanced by the optical gain of the gain cavity, i.e., $\kappa_{\text{eff}} = 0$ [see Eq. (8)]. Meanwhile, as shown in Fig. 3(c), the effective detuning of the loss cavity can be close to the resonant condition with the increase of the measured magnetic field, so that its average photon number also increases significantly. This is in sharp contrast with the inset of Fig. 2(d), where the average photon number is almost unchanged for the magnetic field change of 10^{-10} T. That is to say, at the \mathcal{PT} -symmetry-breaking point, the effect of the measured magnetic field on the system is enhanced significantly. Thus, at the \mathcal{PT} -symmetry-breaking point, the sensitivity of system for the change of the magnetic field is highly enhanced.

V. IMPROVEMENT OF SENSITIVITY OF MAGNETIC-FIELD SENSING

Before improving the sensitivity of the measured weak magnetic field, we should define a sensitivity coefficient η to evaluate the sensing performance of our system. To distinguish each 10^{-11} T of the magnetic-field strength, it is

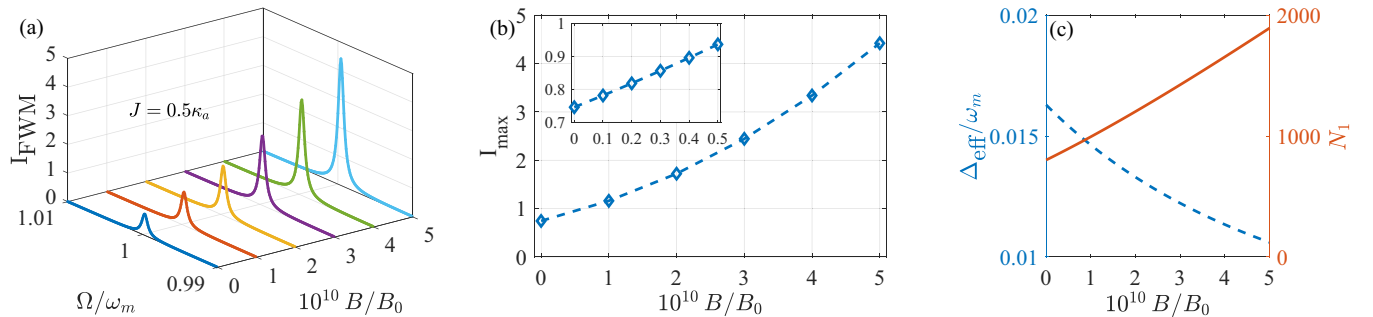


FIG. 3. (a) FWM intensity spectrum as a function of detuning for different measured magnetic fields. (b) Maximum value I_{max} of the FWM intensity as a function of magnetic-field strength. (c) Effective detuning Δ_{eff} and average photon number N_1 of the loss cavity as a function of magnetic-field strength. Parameters are $J = 0.5\kappa_a$, $\Delta_a = 0$, and other parameters are the same as in Fig. 2.

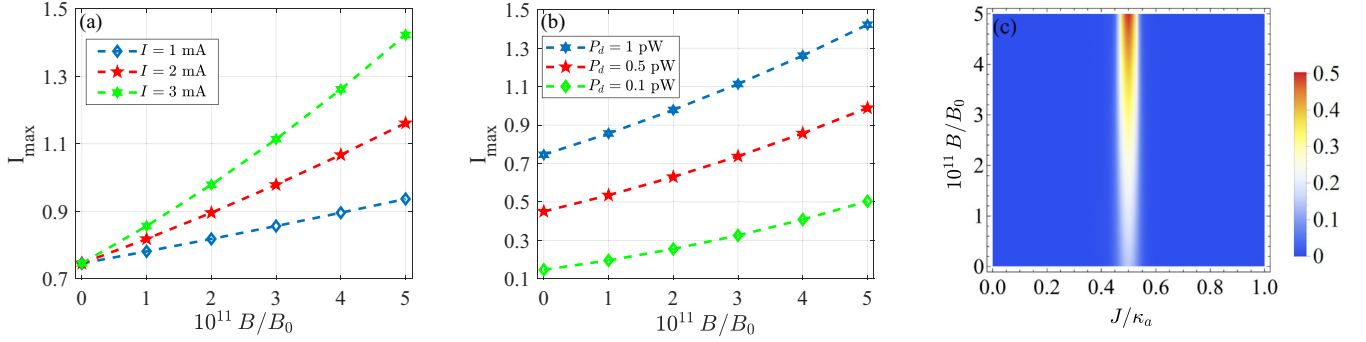


FIG. 4. Maximum value of the FWM intensity as a function of magnetic-field strength for (a) different current intensities I , (b) different driving powers P_d , and (c) different coupling parameters J . Parameters are (a) $P_d = 1$ pW, $I = 1$ mA, 2 mA, and 3 mA; (b) $I = 3$ mA, $P_d = 1$ pW, 0.5 pW, and 0.1 pW; (c) $I = 3$ mA, $P_d = 0.1$ pW. Other parameters are the same as in Fig. 3.

convenient to define the sensitivity coefficient as

$$\eta = \frac{|I_{\max} - I'_{\max}|}{I_{\max} + I'_{\max}} \times 100\%, \quad (23)$$

in which I_{\max} and I'_{\max} represent two adjacent maximum values of the FWM intensity when the magnetic-field strength changes in units of 10^{-11} T. The larger the value of η , the easier it is for us to distinguish the two different FWM intensities.

In our \mathcal{PT} -symmetric COMS, the oscillator is subjected to optomechanical and electromagnetic interactions. To improve the sensitivity of the magnetic-field sensing, we can first increase the interaction between oscillator and magnetic field by increasing the current intensity. As shown in Fig. 4(a), with the increase of the current intensity, each FWM intensity corresponding to the same magnetic-field strength can be enhanced dramatically. On the other hand, we can also decrease the driving power of the loss cavity, which can prevent the electromagnetic interaction from being drowned in the optomechanical interaction. Meanwhile, when the \mathcal{PT} -symmetry-breaking phase occurs, the effective decay rate of the loss cavity is just zero, which can avoid the effects of decay rate on the system under the weak driving condition. As shown in Fig. 4(b), with the decrease of the driving power, although the FWM intensity decreases, its contrast for the change of the magnetic field increases dramatically. Specifically, based on the definition of the sensitivity coefficient η in Eq. (23), the average sensitivity coefficient can be calculated as 6.45%, 7.85%, and 12.24% for the driving power with 1, 0.5, and 0.1 pW. Hence, decreasing the driving power can contribute to enhancing the effect of the \mathcal{PT} -symmetry breaking on the magnetic-field sensing of the system. This is also reflected in Ref. [33], where \mathcal{PT} -symmetry-breaking chaos in

optomechanics was realized with an ultralow driving threshold ($P_d = 0.02$ pW). Moreover, we also analyze the effect of coupling between the gain and loss cavities on the magnetic-field sensing, as shown in Fig. 4(c). One can find that, in the \mathcal{PT} -symmetry-breaking phase (i.e., $J = 0.5\kappa_a$), the contrast for the change in magnetic field is larger than other parameter regions, which also shows that the \mathcal{PT} -symmetry breaking can enhance the performance of the magnetic-field sensing.

VI. CONCLUSIONS

In summary, we have investigated the performance of the \mathcal{PT} -symmetry-breaking enhanced cavity optomechanical magnetometer based on the nonlinear FWM process and analyzed the improvement of sensitivity for the magnetic-field sensing. We showed that, when the \mathcal{PT} -symmetry-breaking phase occurs, the FWM intensity can be enhanced by two orders of magnitude compared with the conventional single loss COMS, meanwhile, the measurement precision can also be increased from 10^{-9} T to 10^{-11} T. Our work uses the combined effects between \mathcal{PT} symmetry and motional sidebands to enhance the performance of cavity optomechanical magnetometers, which is a significant improvement for the magnetometer based on COMSs and will have wide applications in quantum sensing.

ACKNOWLEDGMENTS

This work was supported by the National Key Research and Development Program of China (Grants No. 2017YFA0304202 and No. 2017YFA0205700), the NSFC (Grants No. 11875231 and No. 11935012), and the Fundamental Research Funds for the Central Universities through Grant No. 2018FZA3005.

[1] A. Edelstein, Advances in magnetometry, *J. Phys.: Condens. Matter* **19**, 165217 (2007).
 [2] L. M. Pham *et al.*, Magnetic field imaging with nitrogen-vacancy ensembles, *New J. Phys.* **13**, 045021 (2011).
 [3] L. S. Bouchard, V. M. Acosta, E. Bauch, and D. Budker, Detection of the Meissner effect with a diamond magnetometer, *New J. Phys.* **13**, 025017 (2011).

[4] L. T. Hall *et al.*, Monitoring ion-channel function in real time through quantum decoherence, *Proc. Natl. Acad. Sci. U. S. A.* **107**, 18777 (2010).
 [5] H. B. Dang, A. C. Maloof, and M. V. Romalis, Ultrahigh sensitivity magnetic field and magnetization measurements with an atomic magnetometer, *Appl. Phys. Lett.* **97**, 151110 (2010).

- [6] J. Zhai, Z. Xing, S. Dong, J. Li, and D. Viehland, Detection of pico-tesla magnetic fields using magneto-electric sensors at room temperature, *Appl. Phys. Lett.* **88**, 062510 (2006).
- [7] M. V. Romalis and H. B. Dang, Atomic magnetometers for materials characterization, *Mater. Today (Oxford, U. K.)* **14**, 258 (2011).
- [8] G. Balasubramanian *et al.*, Ultralong spin coherence time in isotopically engineered diamond, *Nat. Mater.* **8**, 383 (2009).
- [9] R. S. Schoenfeld and W. Harneit, Real Time Magnetic Field Sensing and Imaging using a Single Spin in Diamond, *Phys. Rev. Lett.* **106**, 030802 (2011).
- [10] M. Aspelmeyer, T. J. Kippenberg, and F. Marquardt, Cavity optomechanics, *Rev. Mod. Phys.* **86**, 1391 (2014).
- [11] M. Poggio, C. L. Degen, H. J. Mamin, and D. Rugar, Feedback Cooling of a Cantilever's Fundamental Mode below 5 mK, *Phys. Rev. Lett.* **99**, 017201 (2007).
- [12] M. Bhattacharya and P. Meystre, Trapping and Cooling a Mirror to its Quantum Mechanical Ground State, *Phys. Rev. Lett.* **99**, 073601 (2007).
- [13] A. Schliesser, R. Rivière, G. Anetsberger, O. Arcizet, and T. J. Kippenberg, Resolved-sideband cooling of a micromechanical oscillator, *Nat. Phys.* **4**, 415 (2008).
- [14] S. Weis, R. Rivière, S. Deléglise, E. Gavartin, O. Arcizet, A. Schliesser, and T. J. Kippenberg, Optomechanically induced transparency, *Science* **330**, 1520 (2010).
- [15] G. S. Agarwal and S. Huang, Electromagnetically induced transparency in mechanical effects of light, *Phys. Rev. A* **81**, 041803(R) (2010).
- [16] A. Kronwald and F. Marquardt, Optomechanically Induced Transparency in the Nonlinear Quantum Regime, *Phys. Rev. Lett.* **111**, 133601 (2013).
- [17] J. M. Dobrindt, I. Wilson-Rae, and T. J. Kippenberg, Parametric Normal-Mode Splitting in Cavity Optomechanics, *Phys. Rev. Lett.* **101**, 263602 (2008).
- [18] S. Gröblacher, K. Hammerer, M. R. Vanner, and M. Aspelmeyer, Observation of strong coupling between a micromechanical resonator and an optical cavity field, *Nature (London)* **460**, 724 (2009).
- [19] S. Huang and G. S. Agarwal, Normal-mode splitting and anti-bunching in Stokes and anti-Stokes processes in cavity optomechanics: Radiation-pressure-induced four-wave-mixing cavity optomechanics, *Phys. Rev. A* **81**, 033830 (2010).
- [20] Z. C. Zhang, Y. P. Wang, Y. F. Yu, and Z. M. Zhang, Normal-mode splitting in a weakly coupled electromechanical system with a mechanical modulation, *Ann. Phys. (Berlin, Ger.)* **531**, 1800461 (2019).
- [21] S. Forstner, S. Prams, J. Knittel, E. D. van Ooijen, J. D. Swaim, G. I. Harris, A. Szorkovszky, W. P. Bowen, and H. Rubinsztein-Dunlop, Cavity Optomechanical Magnetometer, *Phys. Rev. Lett.* **108**, 120801 (2012).
- [22] H. Xiong, L. G. Si, A. S. Zheng, X. Yang, and Y. Wu, Higher-order sidebands in optomechanically induced transparency, *Phys. Rev. A* **86**, 013815 (2012).
- [23] Z. X. Liu, B. Wang, C. Kong, L. G. Si, H. Xiong, and Y. Wu, A proposed method to measure weak magnetic field based on a hybrid optomechanical system, *Sci. Rep.* **7**, 12521 (2017).
- [24] Z. X. Liu, Precision measurement of magnetic field based on second-order sideband generation in a hybrid electromagnetic-optomechanical system, *IEEE Sens. J.* **18**, 9145 (2018).
- [25] J. Q. Zhang, Y. Li, M. Feng, and Y. Xu, Precision measurement of electrical charge with optomechanically induced transparency, *Phys. Rev. A* **86**, 053806 (2012).
- [26] L. Li, W. X. Yang, Y. Zhang, T. Shui, A. X. Chen, and Z. Jiang, Enhanced generation of charge-dependent second-order sideband and high-sensitivity charge sensors in a gain-cavity-assisted optomechanical system, *Phys. Rev. A* **98**, 063840 (2018).
- [27] Q. Wang, J. Q. Zhang, P. C. Ma, C. M. Yao, and M. Feng, Precision measurement of the environmental temperature by tunable double optomechanically induced transparency with a squeezed field, *Phys. Rev. A* **91**, 063827 (2015).
- [28] J. J. Li and K. D. Zhu, Nonlinear optical mass sensor with an optomechanical microresonator, *Appl. Phys. Lett.* **101**, 141905 (2012).
- [29] Y. He, Sensitivity of optical mass sensor enhanced by optomechanical coupling, *Appl. Phys. Lett.* **106**, 121905 (2015).
- [30] S. W. Bin, X. Y. Lü, T. S. Yin, G. L. Zhu, Q. Bin, and Y. Wu, Mass sensing by quantum criticality, *Opt. Lett.* **44**, 630 (2019).
- [31] V. V. Konotop, J. Yang, and D. A. Zezyulin, Nonlinear waves in \mathcal{PT} -symmetric systems, *Rev. Mod. Phys.* **88**, 035002 (2016).
- [32] H. Jing, S. K. Özdemir, X. Y. Lü, J. Zhang, L. Yang, and F. Nori, \mathcal{PT} -Symmetric Phonon Laser, *Phys. Rev. Lett.* **113**, 053604 (2014).
- [33] X. Y. Lü, H. Jing, J. Y. Ma, and Y. Wu, \mathcal{PT} -Symmetry-Breaking Chaos in Optomechanics, *Phys. Rev. Lett.* **114**, 253601 (2015).
- [34] A. Guo, G. J. Salamo, D. Duchesne, R. Morandotti, M. Volatier-Ravat, V. Aimez, G. A. Siviloglou, and D. N. Christodoulides, Observation of \mathcal{PT} -Symmetry Breaking in Complex Optical Potentials, *Phys. Rev. Lett.* **103**, 093902 (2009).
- [35] B. Peng, K. Özdemir, S. Rotter, H. Yilmaz, M. Liertzer, F. Monifi, C. M. Bender, F. Nori, and L. Yang, Loss-induced suppression and revival of lasing, *Science* **346**, 328 (2014).
- [36] H. Hodaei, M.-A. Miri, M. Heinrich, D. N. Christodoulides, and M. Khajavikhan, Parity-time-symmetric microring lasers, *Science* **346**, 975 (2014).
- [37] L. Feng, Z. J. Wong, R. M. Ma, Y. Wang, and X. Zhang, Single-mode laser by parity-time symmetry breaking, *Science* **346**, 972 (2014).
- [38] R. Fleury, D. Sounas, and A. Alu, An invisible acoustic sensor based on parity-time symmetry, *Nat. Commun.* **6**, 5905 (2015).
- [39] Z. P. Liu, J. Zhang, K. Özdemir, B. Peng, H. Jing, X. Y. Lü, C. W. Li, L. Yang, F. Nori, and Y. X. Liu, Metrology with \mathcal{PT} -Symmetric Cavities: Enhanced Sensitivity near the \mathcal{PT} -Phase Transition, *Phys. Rev. Lett.* **117**, 110802 (2016).
- [40] M. Zhang, W. Sweeney, C. W. Hsu, L. Yang, A. D. Stone, and L. Jiang, Quantum Noise Theory of Exceptional Point Amplifying Sensors, *Phys. Rev. Lett.* **123**, 180501 (2019).
- [41] L. Y. He, Parity-time-symmetry-enhanced sideband generation in an optomechanical system, *Phys. Rev. A* **99**, 033843 (2019).
- [42] T. J. Kippenberg, S. M. Spillane, and K. J. Vahala, Kerr-Nonlinearity Optical Parametric Oscillation in an Ultrahigh- Q Toroid Microcavity, *Phys. Rev. Lett.* **93**, 083904 (2004).
- [43] E. M. Graefe, H. J. Korsch, and A. E. Niederle, Quantum-classical correspondence for a non-Hermitian Bose-Hubbard dimer, *Phys. Rev. A* **82**, 013629 (2010).
- [44] H. Ramezani, T. Kottos, R. El-Ganainy, and D. N. Christodoulides, Unidirectional nonlinear \mathcal{PT} -symmetric optical structures, *Phys. Rev. A* **82**, 043803 (2010).

- [45] C. Gardiner, P. Zoller, and P. Zoller, *Quantum Noise: A Handbook of Markovian and Non-Markovian Quantum Stochastic Methods with Applications to Quantum Optics* (Springer, New York, 2004).
- [46] J. D. Thompson, B. M. Zwickl, A. M. Jayich, F. Marquardt, S. Girvin, and J. G. E. Harris, Strong dispersive coupling of a high-finesse cavity to a micromechanical membrane, [Nature \(London\) **452**, 72 \(2008\)](#).